Supplement of

Precessional pacing of tropical ocean carbon export during the Late Cretaceous

Ji-Eun Kim et al.

Correspondence to:

Elizabeth M. Griffith (griffith.906@osu.edu) and Thomas Westerhold (twesterhold@marum.de)

This PDF file includes:

Supplementary text S1-S2
Figures S1 to S15
Tables S1 to S5
Captions for Datasets S1-S16

Other supplementary materials for this manuscript include the following:

Datasets S1 to S16

Supplementary Information Text

S1 - Excess-Ba corrections

Because Ba content in deep sea sediments can have non-biogenic sources (e.g., riverine sources), studies that use Ba as an export production proxy typically correct for any possible terrestrial input of Ba in the bulk sample measurement by measuring Al which is primarily from terrigenous sources. Equation (Eq 1) from Dymond et al. (1992) is used in this study with the $Ba/Al_{terrigenous}$ ratio of 0.0037 after Reitz et al. (2004).

$$\text{(Eq 1)}\ [Ba_{excess}]_{ppm} = [Ba_{total}]_{ppm} - \left(Ba/Al_{terrigenous}\right) \times [Al_{total}]_{ppm}$$

Additional corrections for non-biogenic Ba in deep sea sediments associated with authigenic components and Fe-smectite were suggested by Olivarez-Lyle and Lyle (2006). Here we compared the two corrections to see if the excess-Ba signal is significantly impacted by additional non-biogenic Ba sources using Mn and Fe measurements, and a $Ba/Mn_{authigenic}$ ratio of 0.014 and $Ba/Fe_{Fe\text{-}smectite}$ ratio of 0.02, respectively.

$$\text{(Eq 2)}\ [Ba_{excess}]_{ppm} = [Ba_{total}]_{ppm} - \left[\left(Ba/Al_{terrigenous} \times [Al_{total}]_{ppm}\right) + \left(Ba/Mn_{authigenic} \times [Mn_{total}]_{ppm}\right) + \left(Ba/Fe_{Fe-smectite} \times [Fe_{total}]_{ppm}\right)\right]$$

The average corrected Ba_{excess} is 0.497 mg kyr^{-1} cm^{-2} using equation (1) and 0.487 mg kyr^{-1} cm^{-2} using equation (Eq 2) for the 51 excess-Ba calculations or approximately 2% different (Data set S15). This difference between two corrections does not impact our results, so the more common Al only correction is used in this study.

S2 – New production calculation

New production (Pnew) was calculated following Dymond et al. (1992) using excess-BaAR and a conservative Ba value from 1700 m of 110 µmol kg^{-1} from the southwest tropical Pacific, which is close to the approximate depth of Shatsky Rise during the Maastrichtian, although the actual Ba concentration at midwater depths at this time are unknown. Values ranged from 0.5 to 2.2 g C cm^{-2} yr^{-1} (Data set S15) and are relatively low when compared to modern Pacific core top sediments ranging between 1 and 43 g C cm^{-2} yr^{-1} (Eagle et al., 2003).

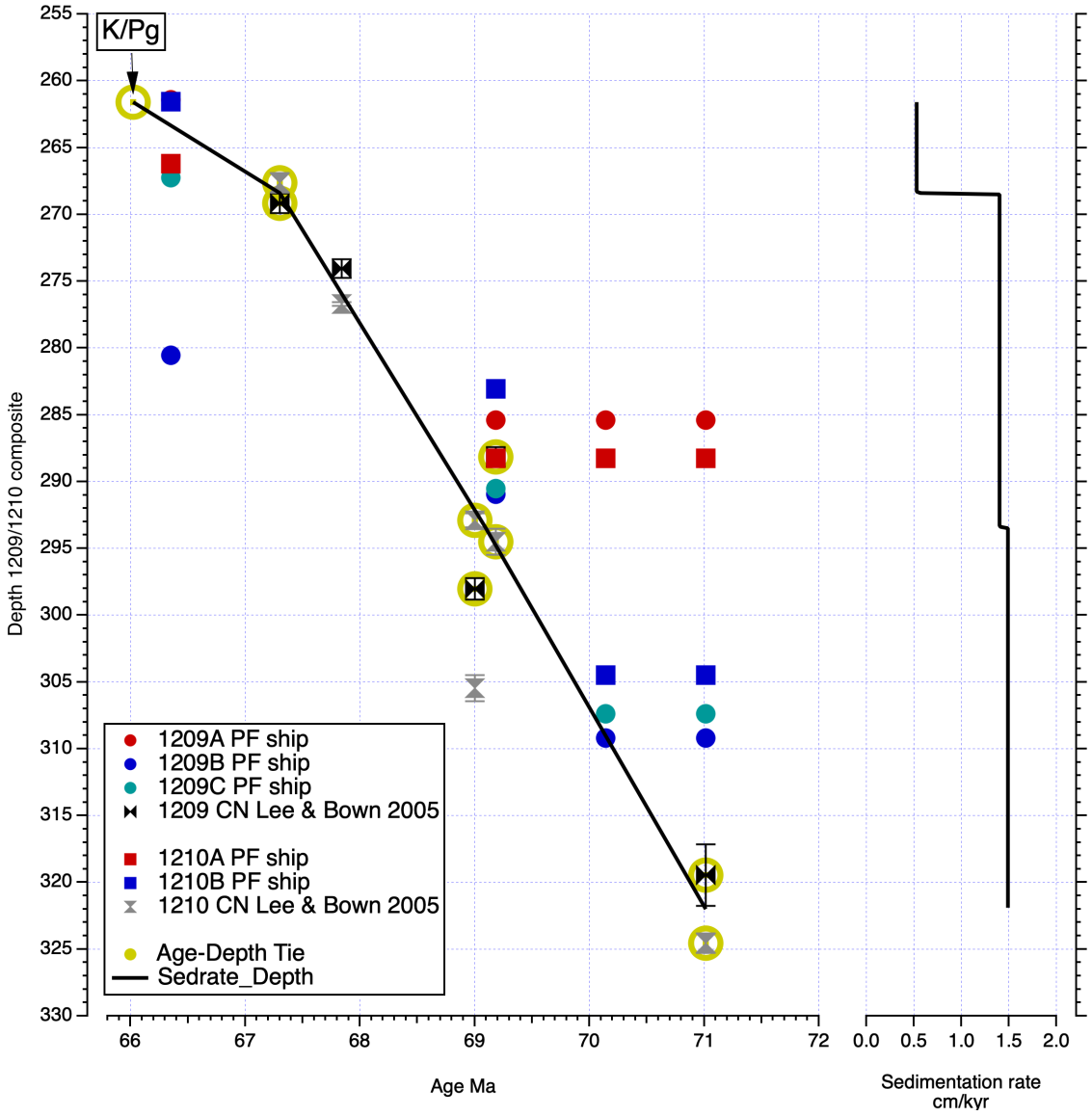

Figure S1. Age vs depth plot using the shipboard biostratigraphic datums. PF = planktonic foraminiferal datums, CN = calcareous nannofossil datums. Note the widespread for planktonic foraminifera datums suggesting uncertain calibration and age estimates for those events in the literature. Inconsistencies also exist using calcareous nannofossil datums reflecting issues in the concept of classification as well. The preferred option used here for sedimentation rate calculation to be able to identify orbital cycles is in line with the interpretations given by Jung et al. (2012) and Dameron et al. (2017).

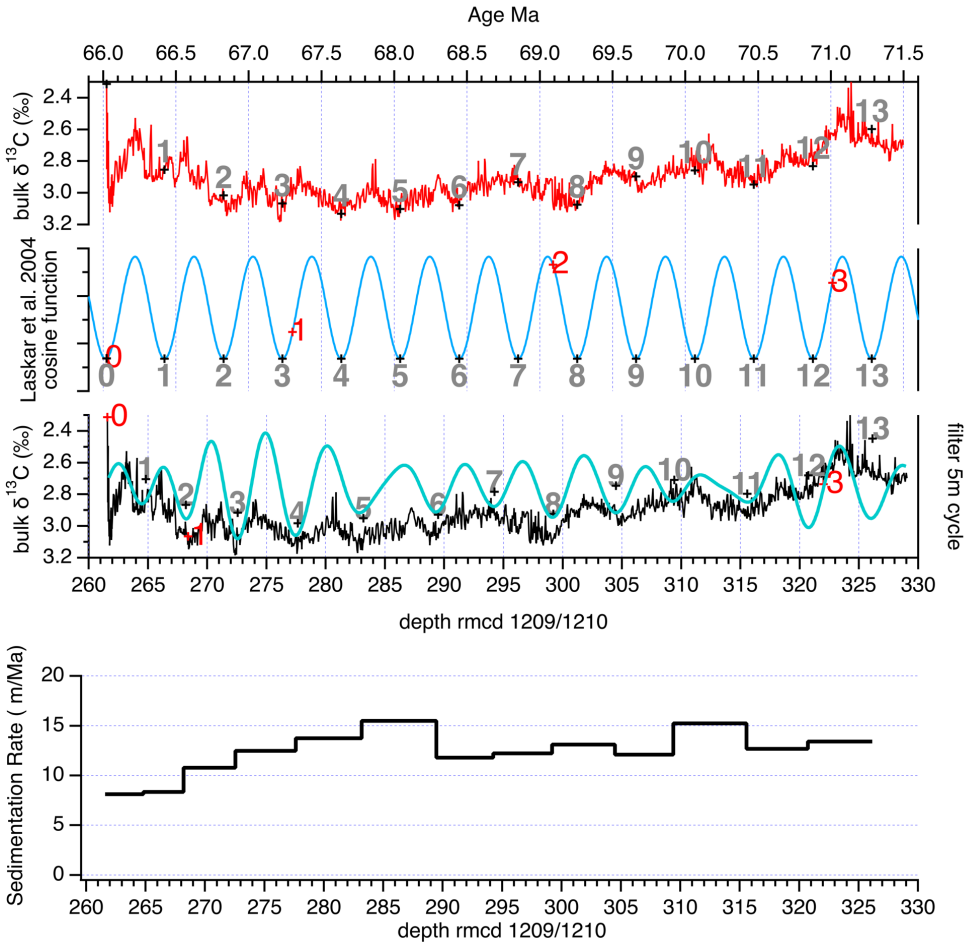

Figure S2. (top) Basic 405 kyr age model was first made by assigning Shatsky Rise Sites 1209 and 1210 composite bulk $\delta^{13}C$ to known tie points (red numbers). Then, 5 m filter (bandpass 0.2 ± 0.06) of bulk $\delta^{13}C$ composite was modelled to know the cosine function (cyan line). This cosine function was correlated to La2004 Cosine function (Laskar et al., 2004; blue line) minima for tuning the depth to the stable 405 kyr cycle for an age. New age is tie points in Table S1. (bottom) Sedimentation rate of composite depth.

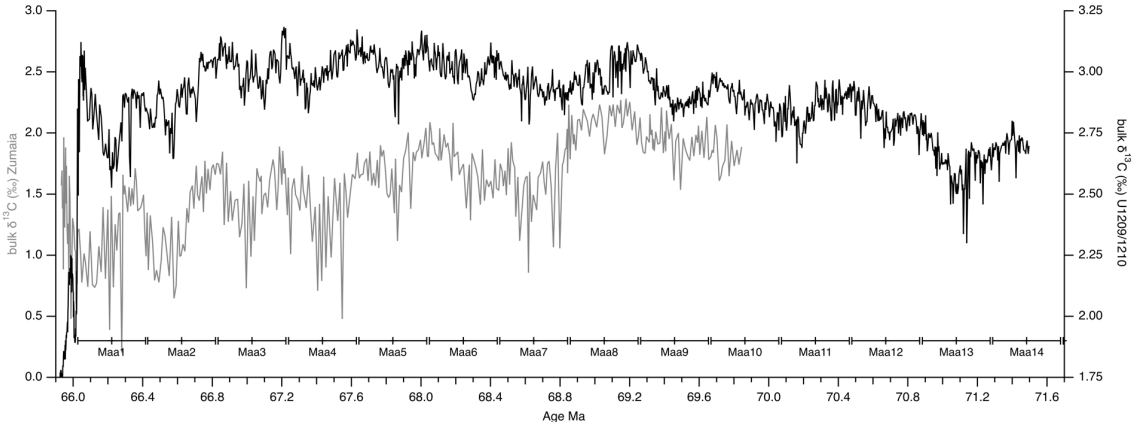

Figure S3. Comparison of the Zumaia bulk $\delta^{13}C$ (grey line; Batenburg et al., 2012, 2014) from mid-latitude Atlantic with the new Shatsky Rise Sites 1209 and 1210 composite bulk $\delta^{13}C$ (black line; this study). Zumaia age tie points in Table S2. Note age is increasing from the left to right.

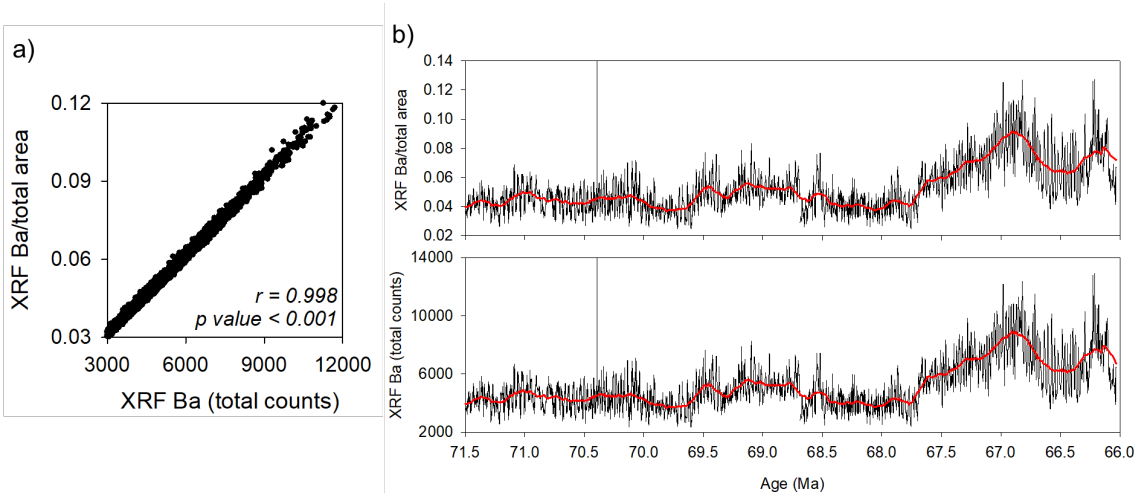

Figure S4. (a) Relationship between XRF Ba (total counts) and XRF Ba/total area with a r value of 0.998 and significant p value < 0.001. (b) XRF Ba/total area and XRF Ba (total counts) vs age in millions of years ago (Ma) show identical trends. Note age is decreasing from left to right.

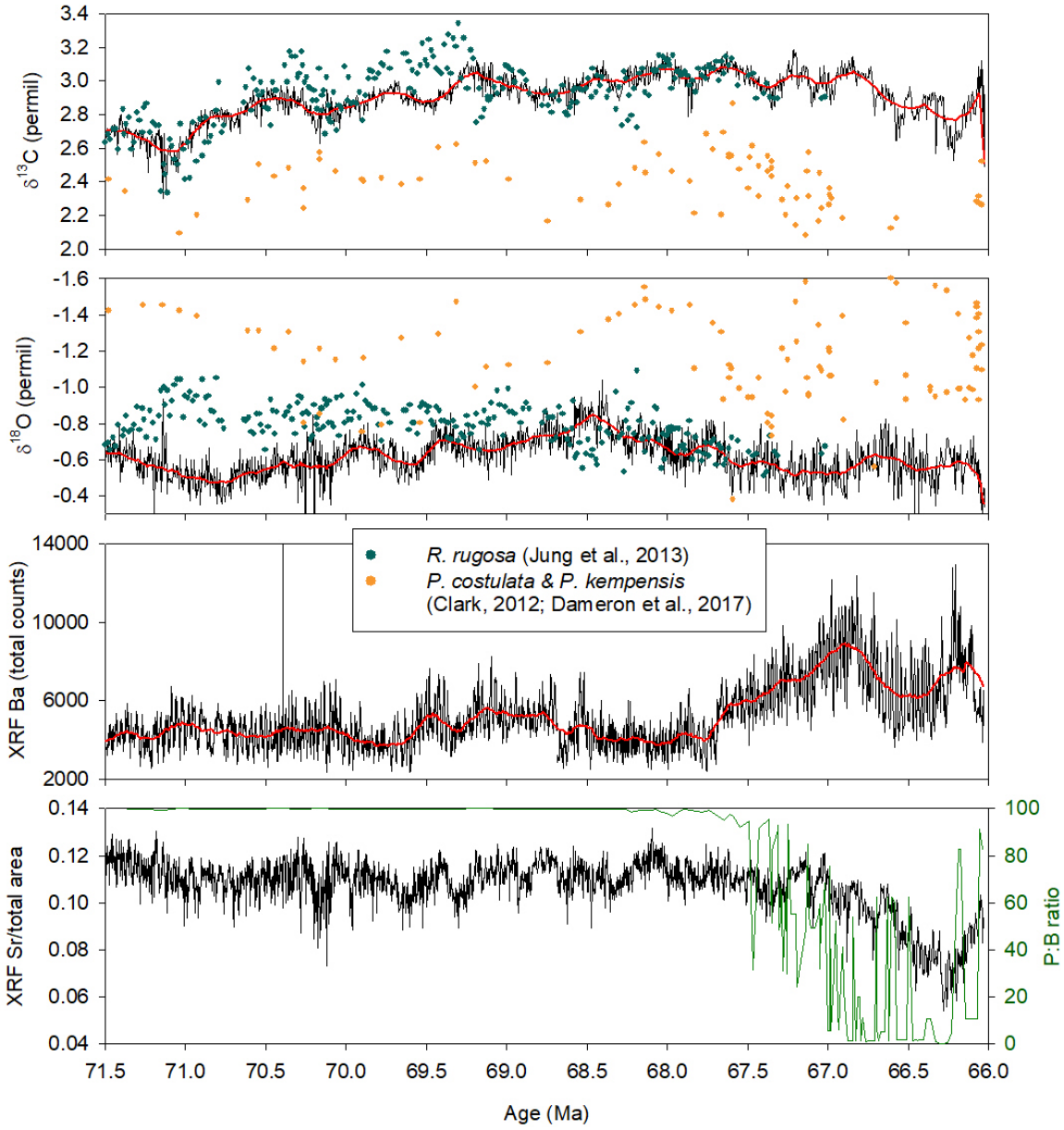

Figure S5. (from top to bottom) Shatsky Rise composite bulk $\delta^{13}C$ (black line) with 50 points moving average (red line) shown with planktic foraminifera $\delta^{13}C$ from *Rugoglobigerina rugosa* (Jung et al., 2013; green circles) and planktic foraminifera $\delta^{13}C$ from *Pseudoguembelina costulata* and *P. kempensis* (Clark et al., 2012; Dameron et al., 2017; orange circles). Shatsky Rise composite bulk $\delta^{18}O$ (black line) with planktic foraminifera $\delta^{18}O$. XRF Ba (total counts) with 100 points moving average (red line). At the bottom, XRF Sr/total area is plotted with planktic:benthic foraminifera ratio (P:B ratio; Dameron et al., 2017) in green. Note age is decreasing from the left to right.

a.

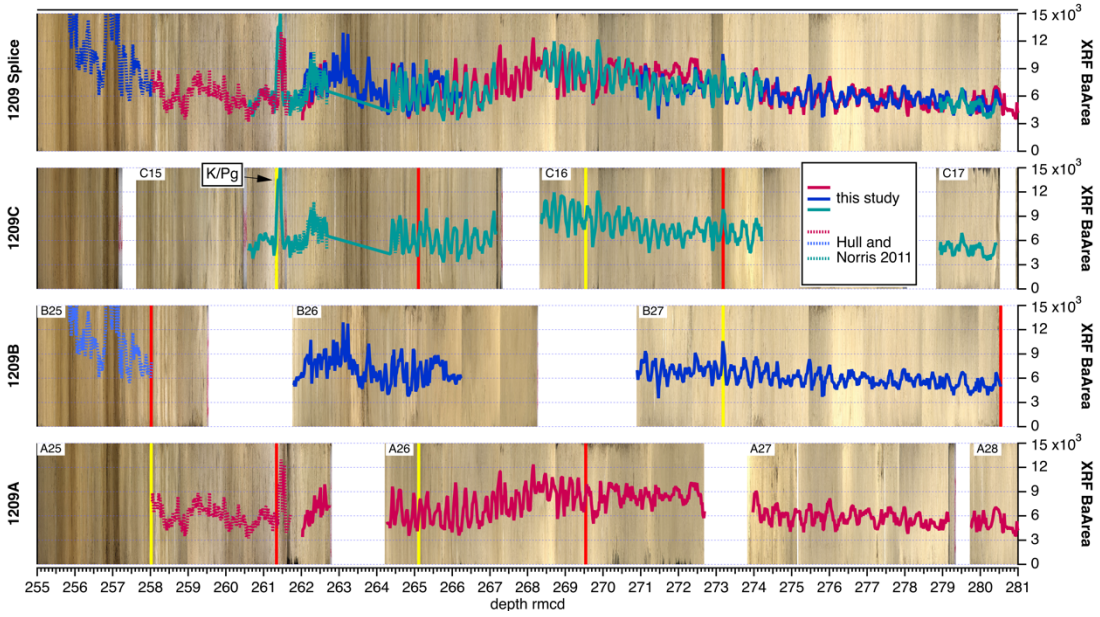

b.

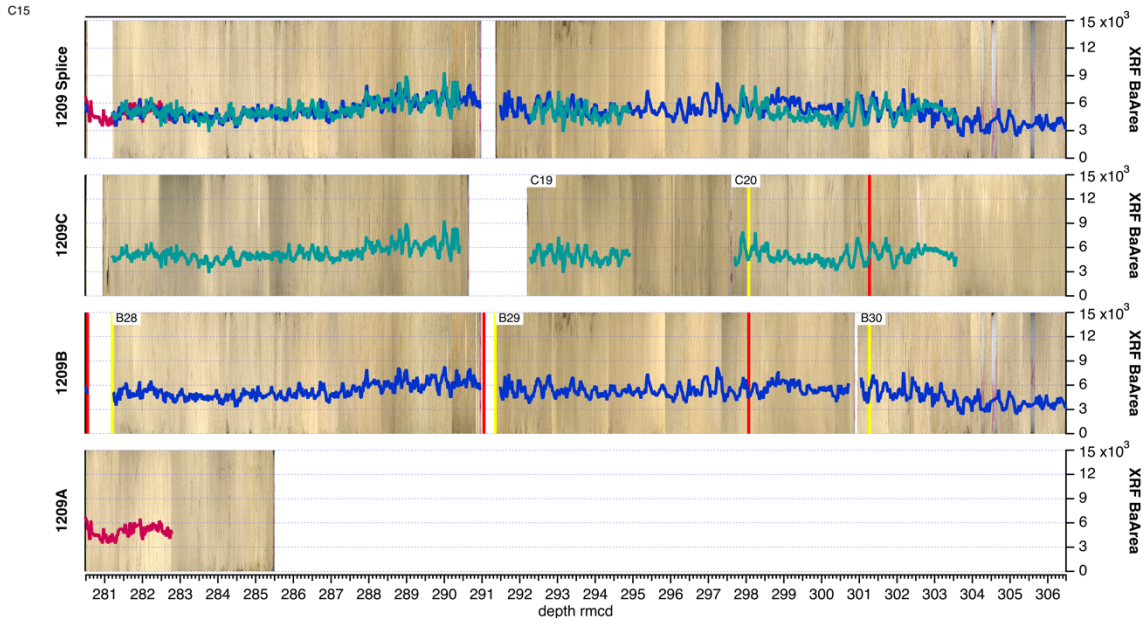

Figure S6. New composite for ODP Site 1209 based on XRF Ba elemental data. (a) from depth 255 rmcd to 281 rmcd, (b) from depth 280 to 307 rmcd, and (c) from depth 305 to 330 rmcd.

c.

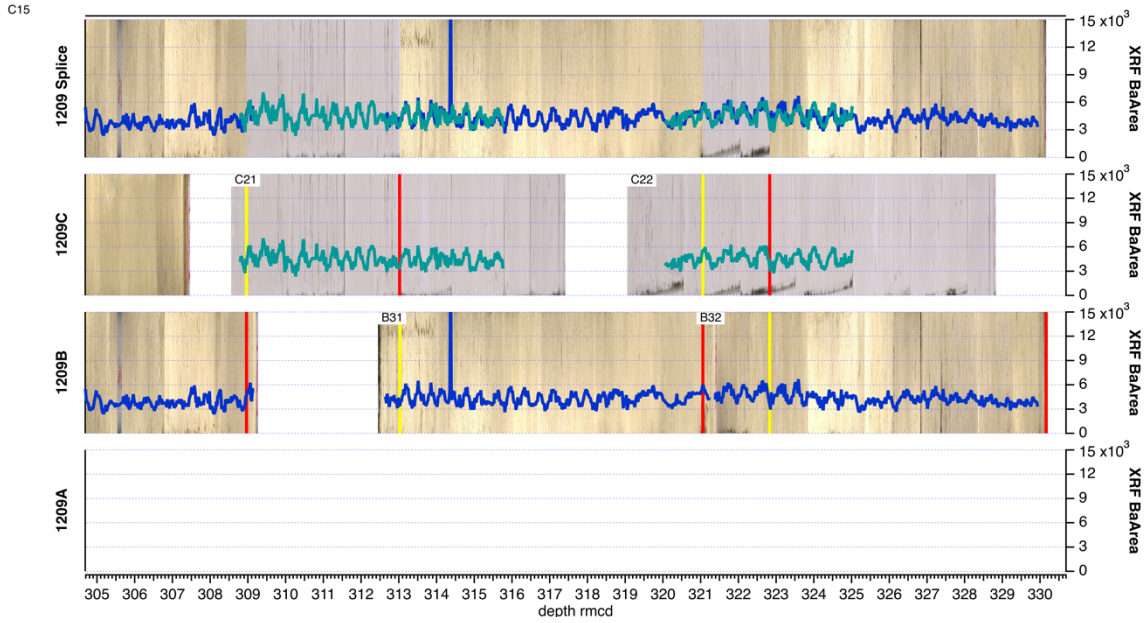

Figure S6c. New composite for ODP Site 1209 based on XRF Ba elemental data – continued.

a.

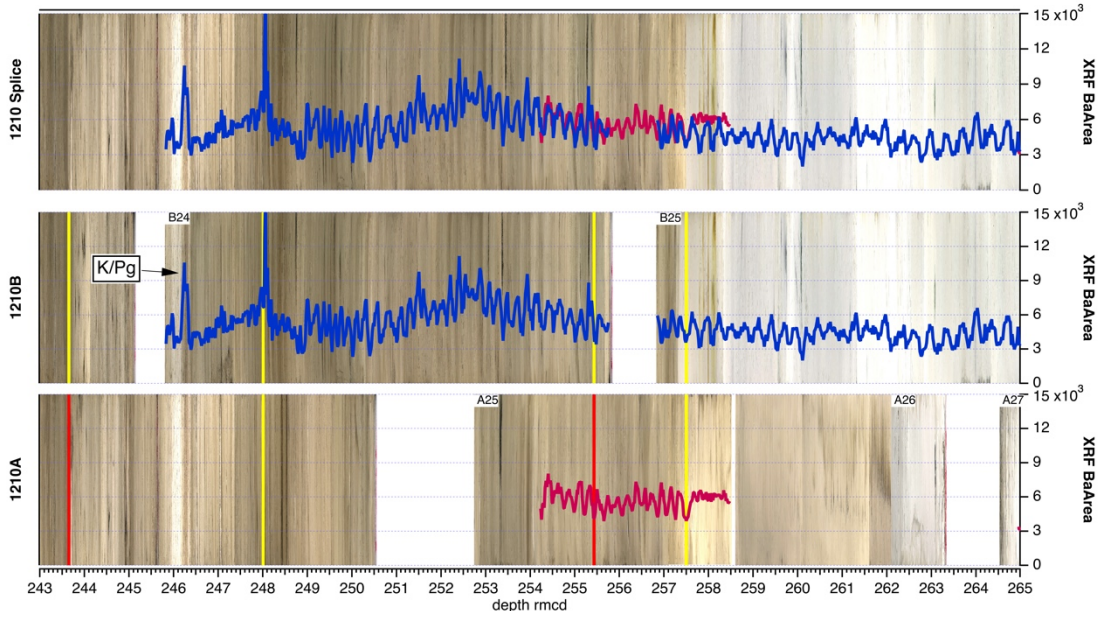

b.

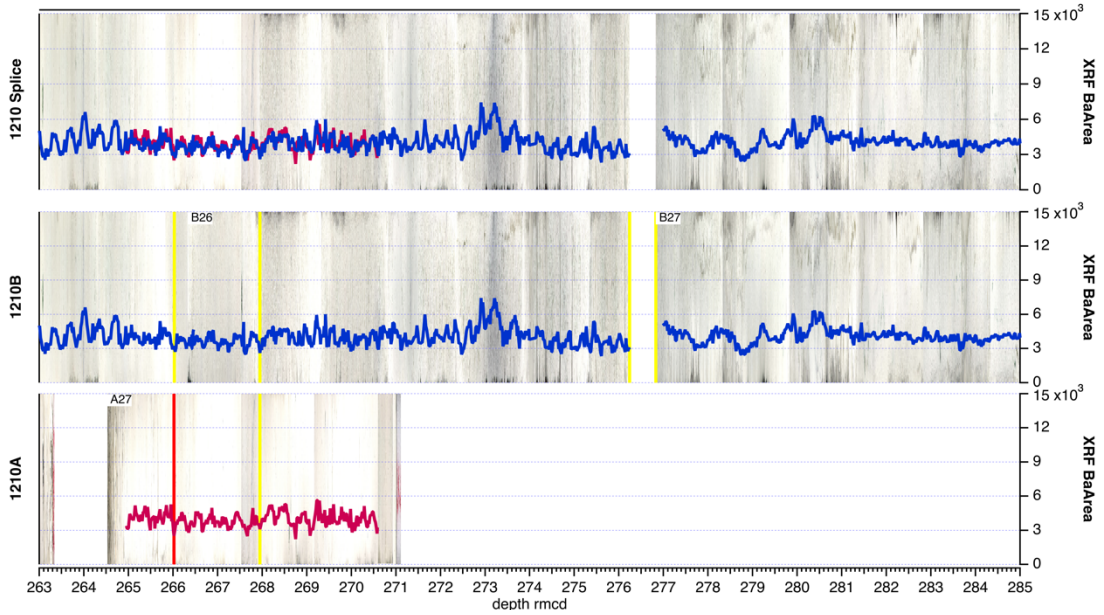

Figure S7. New composite for ODP Site 1210 based on XRF Ba elemental data. (a) from depth 243 rmcd to 265 rmcd, (b) from depth 263 to 285 rmcd, (c) from depth 283 to 305 rmcd, and (d) from 299 to 320 rmcd.

c.

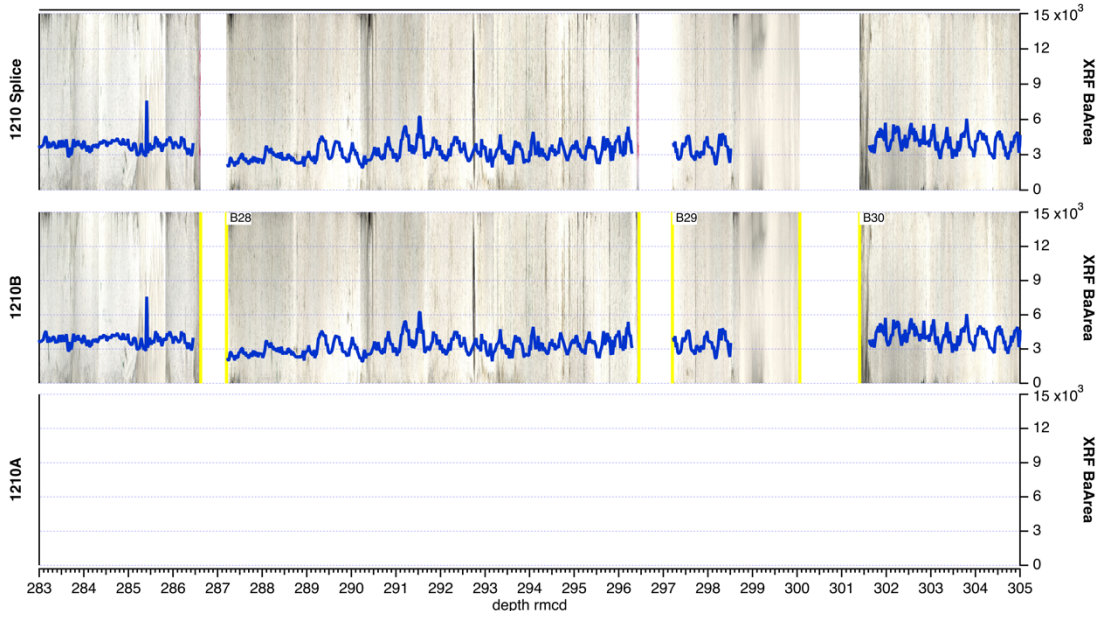

d.

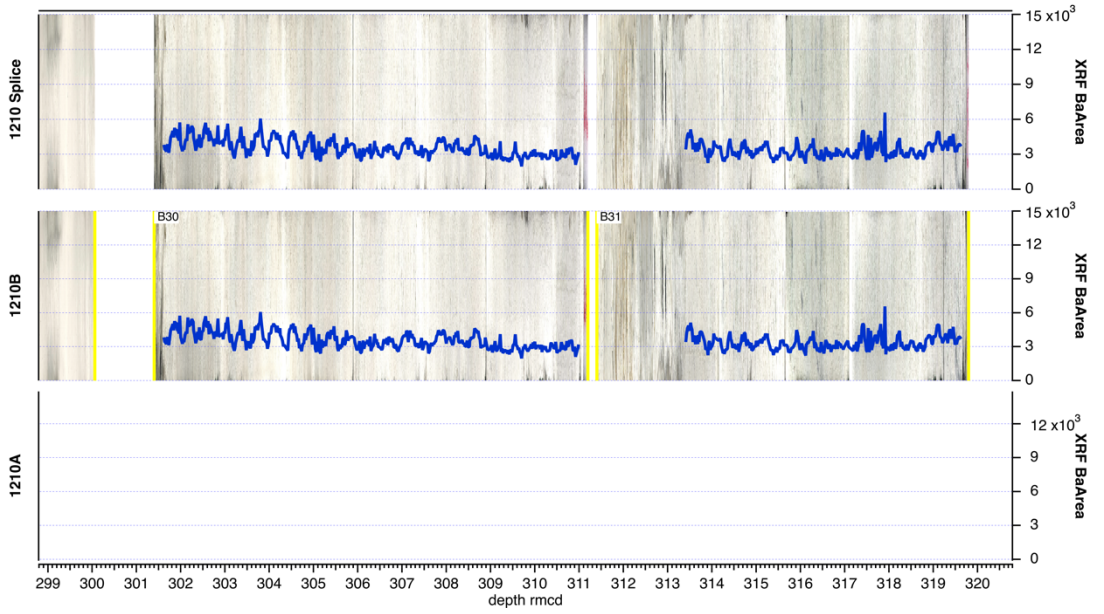

Figure S7c-d. New composite for ODP Site 1210 based on XRF Ba elemental data – continued.

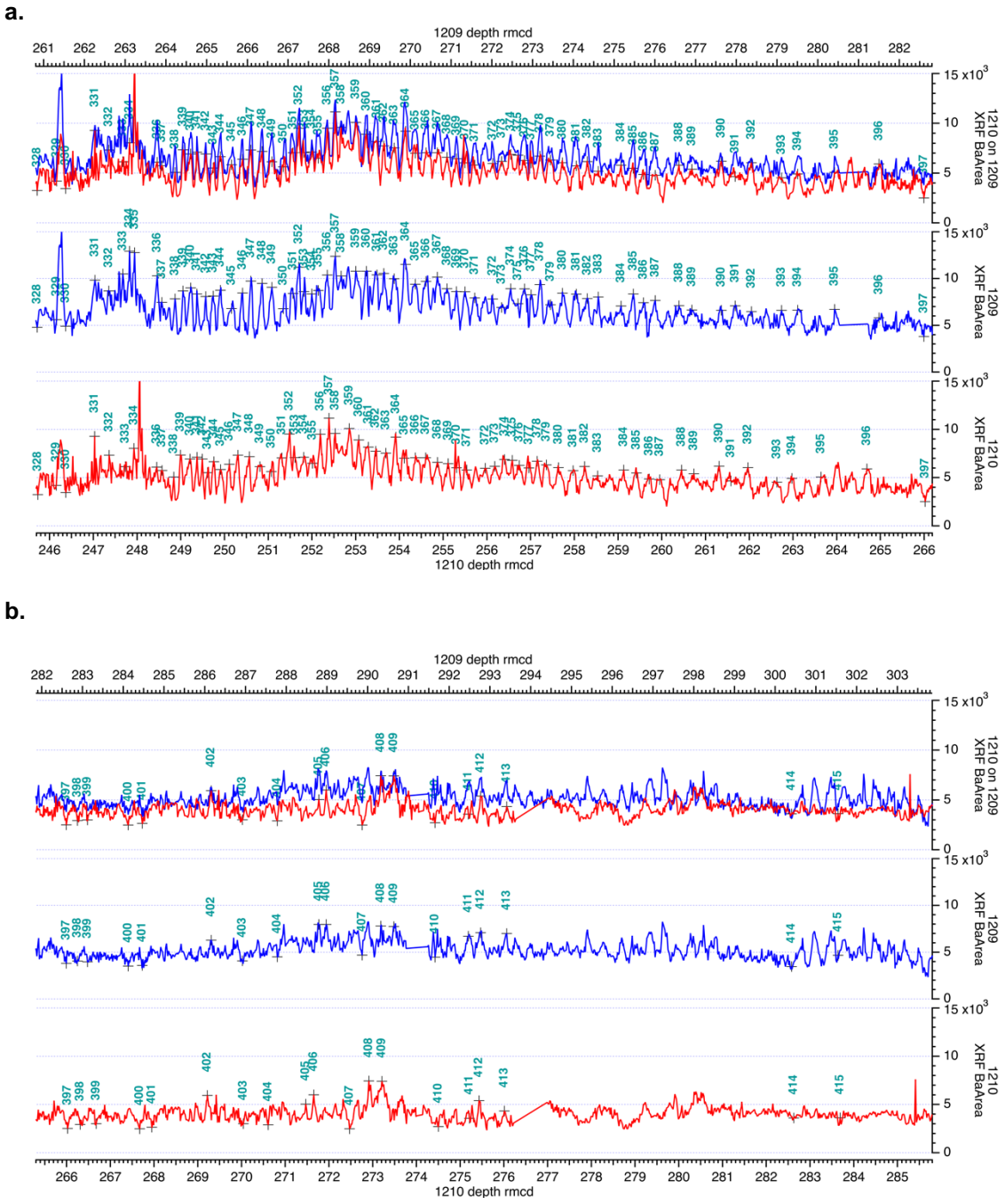

Figure S8. Correlation between ODP Sites 1209 and 1210 new composite records. Numbers represent tie points and are given in Dataset S13 for the entire two sites. Relevant here are the tie points starting at the K/Pg (#330) into the Maastrichtian (up to # 447).

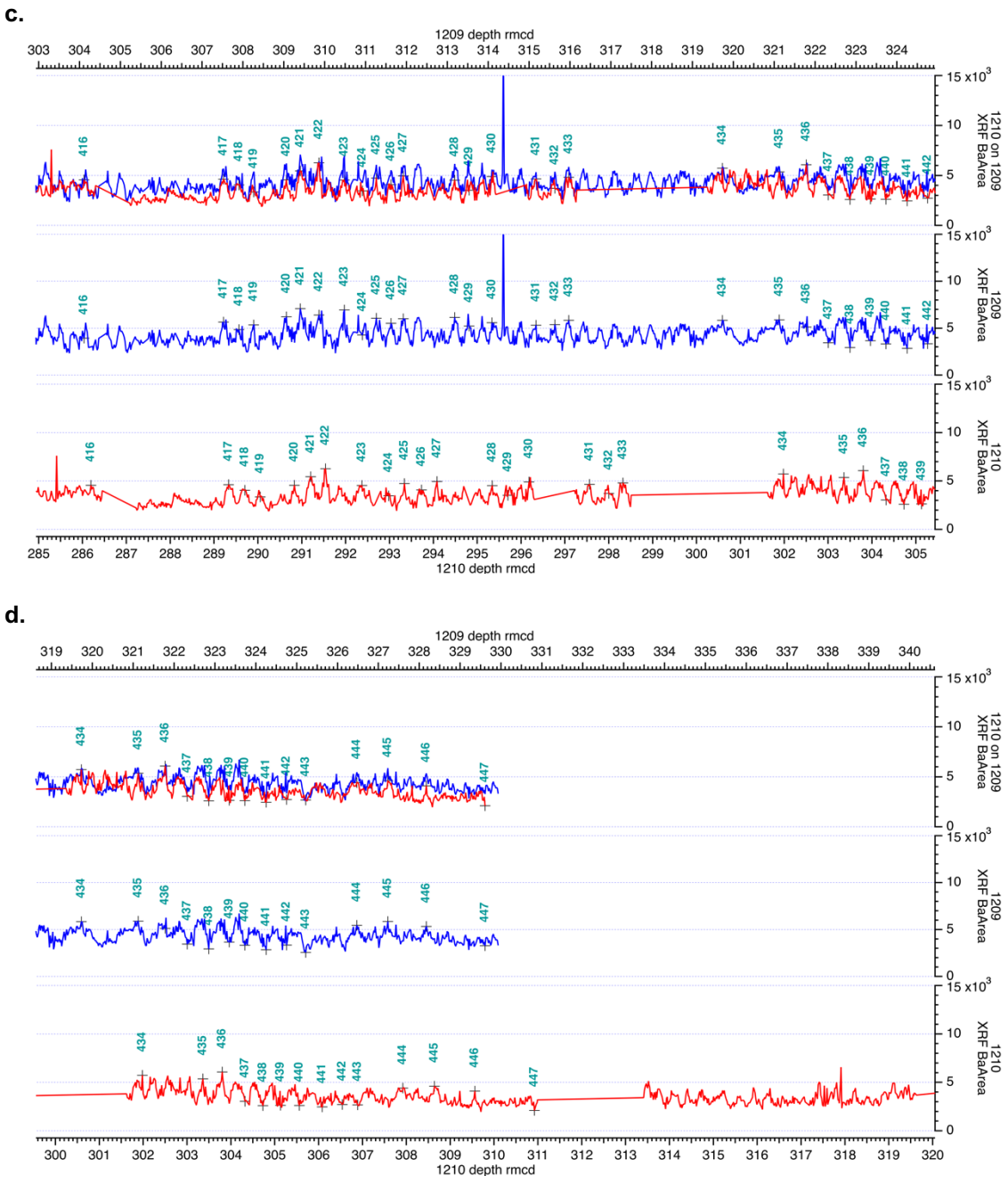

Figure S8c-d. Correlation between ODP Sites 1209 and 1210 new composite records – continued.

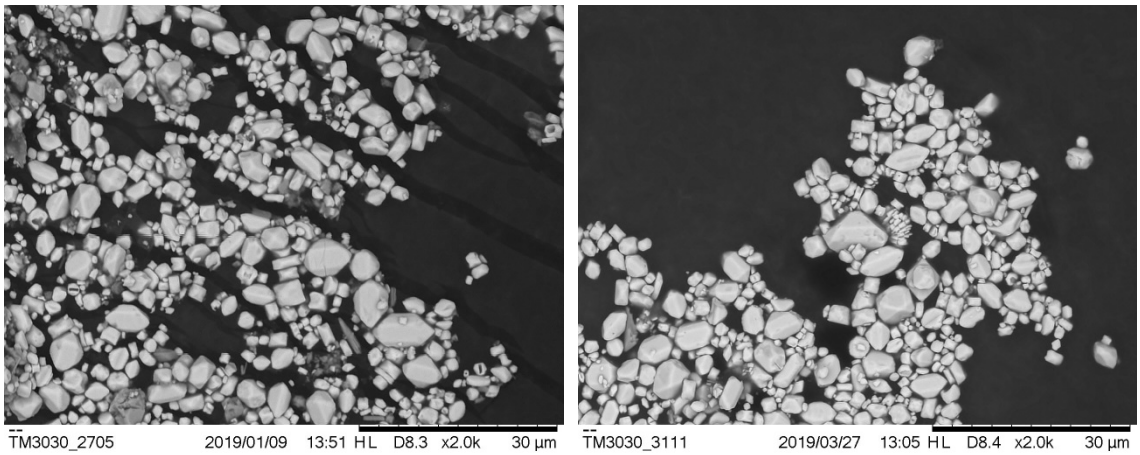

Figure S9. (left) Barite SEM image from 1209C 16H 1W 137 to 139 cm (x2000) with 91.9% barite in the residue after extraction and (right) 1209C 22H 3W 8 to 10 cm (x2000) with 96.1% barite in the residue after extraction. Both are typical of marine pelagic barite formed in microenvironments within the water column that have close relationship to organic carbon export. White euhedral minerals are barite and darker grey-tone minerals are mostly rutile.

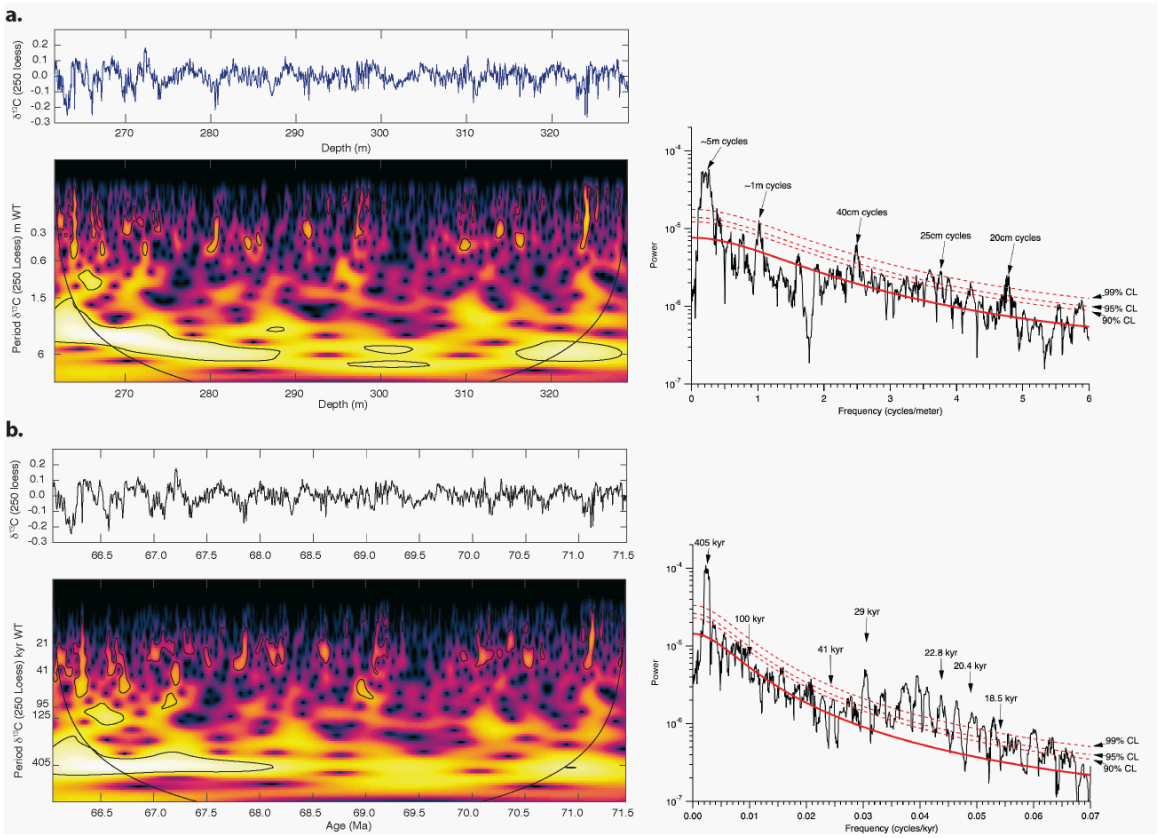

Figure S10. (top) Bulk carbonate $\delta^{13}C$ by depth shown with 250-point LOESS smoothing and wavelet analysis, and multi-taper method (MTM) shown for spectral analysis. (bottom) $\delta^{13}C$ by age (ka) shown with 250-point LOESS smoothing and wavelet analysis, and MTM shown for spectral analysis. CL indicates confidence level. Note age is increasing from the left to right.

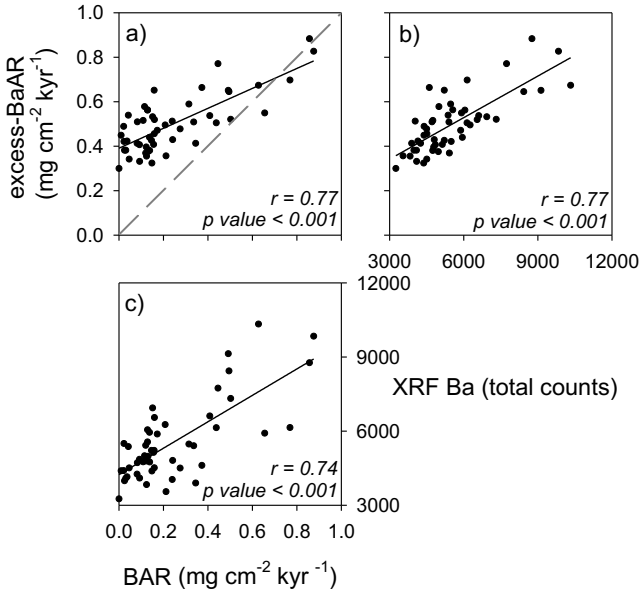

Figure S11. Marine pelagic barite accumulation rate (BAR), excess-Ba accumulation rate (excess-BaAR), and XRF Ba (total counts) compared to each other. All correlations between barite related proxies were significant ($p < 0.001$).

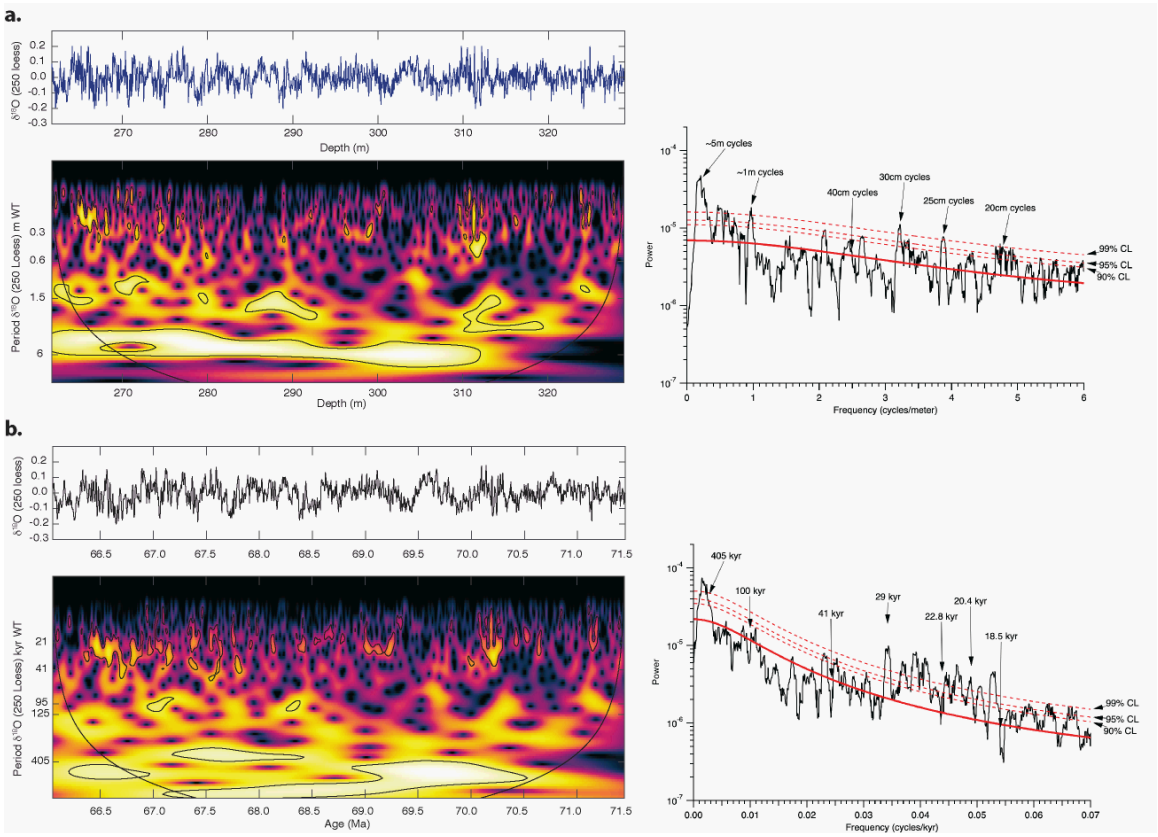

Figure S12. (top) Bulk carbonate $\delta^{18}O$ by depth shown with 250-point LOESS smoothing and wavelet analysis, and multi-taper method (MTM) shown for spectral analysis. (bottom) $\delta^{18}O$ by age (ka) shown with 250-point LOESS smoothing and wavelet analysis, and MTM shown for spectral analysis. CL indicates confidence level. Note age is increasing from the left to right.

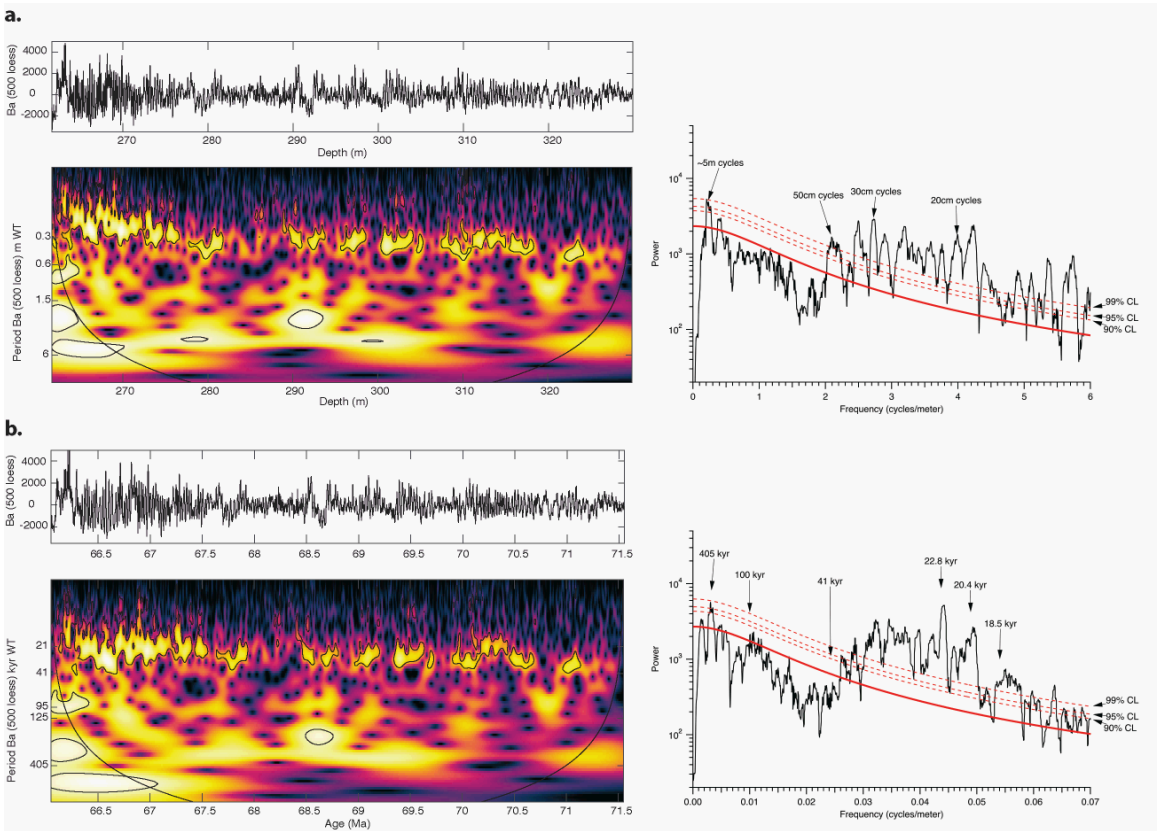

Figure S13. (top) XRF Ba by depth shown with 500-point LOESS smoothing and wavelet analysis, and multi-taper method (MTM) shown for spectral analysis. (bottom) XRF Ba by age (ka) shown with 500-point LOESS smoothing and wavelet analysis, and MTM shown for spectral analysis. CL indicates confidence level. Note age is increasing from the left to right.

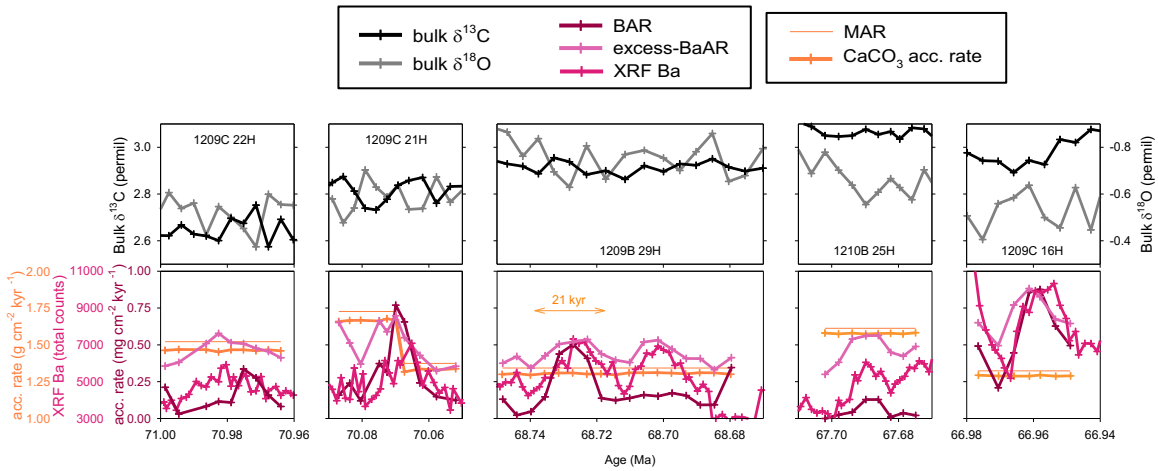

Figure S14. Bulk carbonate $\delta^{13}C$ (black) and $\delta^{18}O$ (gray) from five selected windows of time, from oldest (left) to youngest (right). Bulk mass accumulation rate (MAR) and $CaCO_3$ accumulation rate shown as thin and thick orange lines, respectively. Barium accumulation rates are shown in pink (see legend). Refer to Data sets S10, S13-S15.

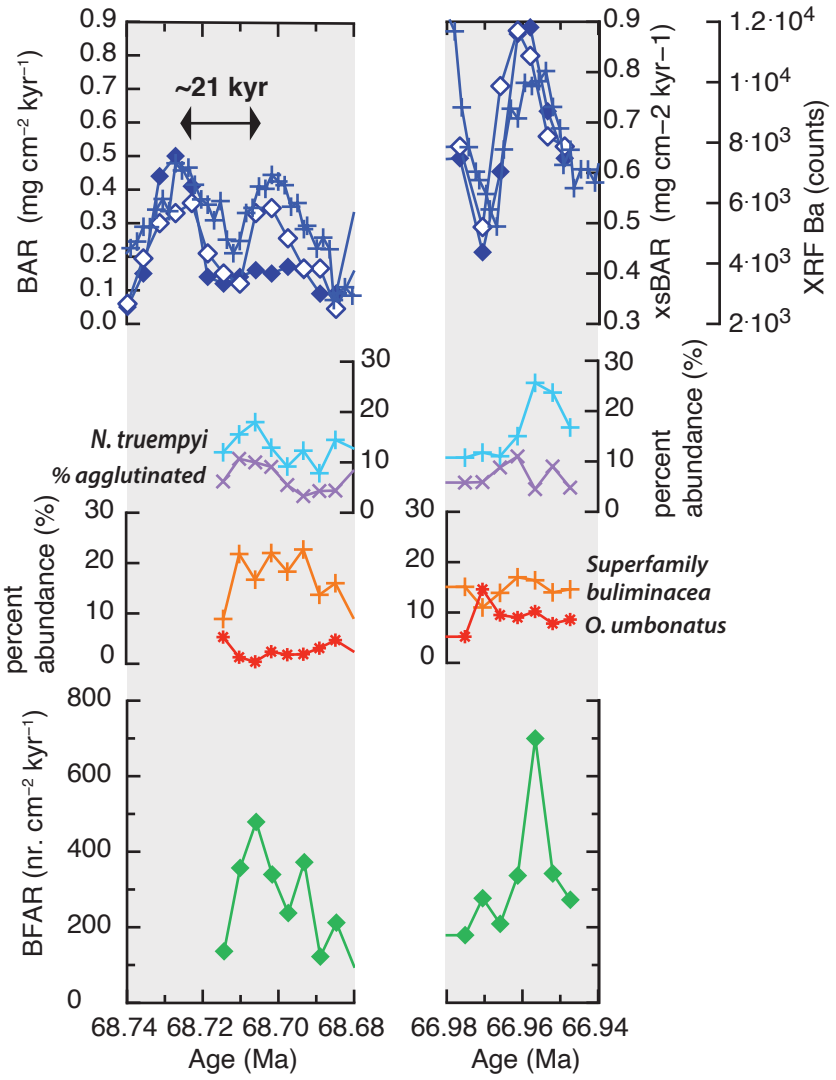

Figure S15. Two discrete sample intervals with organic carbon export proxies (XRF Ba = crosses, excess-BaAR = open diamonds, and BAR = solid diamonds), and organic carbon arrival at the seafloor proxies (BFAR = green diamond) with benthic foraminiferal abundances (*N. truempyi* = light blue croses, *% agglutinated = purple x's, % Superfamily buliminacea = orange crosses, % O. umbonatus = red stars*). Refer to Data sets S15-S16. Age decreasing from left to right.

Table S1. Leg 198 Sites 1209 and 1210 basic 405 kyr age model.

Depth 1209_1210 composite, rmcd (m)	Age (Ma)	Age Tie ID
261.580	66.022	K/Pg boundary
264.810	66.420	La2004CosineFunction Minimum; start Maa1
268.200	66.826	La2004CosineFunction Minimum; start Maa2
272.560	67.230	La2004CosineFunction Minimum; start Maa3
277.630	67.636	La2004CosineFunction Minimum; start Maa4
283.188	68.040	La2004CosineFunction Minimum; start Maa5
289.474	68.446	La2004CosineFunction Minimum; start Maa6
294.240	68.850	La2004CosineFunction Minimum; start Maa7
299.200	69.256	La2004CosineFunction Minimum; start Maa8
304.495	69.660	La2004CosineFunction Minimum; start Maa9
309.410	70.066	La2004CosineFunction Minimum; start Maa10
315.570	70.470	La2004CosineFunction Minimum; start Maa11
320.720	70.876	La2004CosineFunction Minimum; start Maa12
326.140	71.280	La2004CosineFunction Minimum; start Maa13

Table S2. Zumaia 405 kyr age model tie points.

Depth (m)	Age Ma	Age Tie ID
0	66.022	K/Pg boundary
16	66.42	La2004CosineFunction Minimum; start Maa1
32	66.826	La2004CosineFunction Minimum; start Maa2
47	67.23	La2004CosineFunction Minimum; start Maa3
61	67.636	La2004CosineFunction Minimum; start Maa4
76	68.04	La2004CosineFunction Minimum; start Maa5
91	68.446	La2004CosineFunction Minimum; start Maa6
111	68.85	La2004CosineFunction Minimum; start Maa7
122	69.256	La2004CosineFunction Minimum; start Maa8
135	69.66	La2004CosineFunction Minimum; start Maa9

Table S3. Barite separation method modified from Paytan et al. (1996).

Step	Description
	Weigh 14-20 g of sample into 500 ml Nalgene bottle
2	Dissolve carbonates with 25% acetic acid in 1 L beaker and transfer sample back to Nalgene bottle after reaction stops. Leave at room temperature with caps loose overnight
3	Perform three deionized water rinses in centrifuge at 3000 rpm for 10 minutes
4	Dissolve organics with bleach and leave at 50°C with caps loose overnight in Nalgene bottle. Rinse.
5	Dissolve Fe-Mn oxyhydroxides with 0.02N hydroxylamine in acetic acid and leave at 80°C with caps loose overnight. Rinse and transfer sample to 50 ml falcon tube.
6	Dissolve silicates with 30 ml of 1:2 HF:HNO_3 (1N) and leave at room temperature with caps loose overnight. Rinse.
7	If silicate is still present, dissolve with 1:1 HF:HNO_3 (1N) and leave at room temperature overnight. Rinse. If needed, follow up with 2:1 HF:HNO_3 (1N) and repeat.
8	Dissolve fluorides with 15 ml of saturated aluminum chloride (in 1N nitric acid). Leave at 80°C oven for 1 hour with caps loose.
9	Filter residue on to 0.4 μm filter paper with known weight. Dry residue overnight and weigh.
10	Examine under SEM for barite purity. Correct residue weight for any impurities.

Table S4. Bulk digestion method modified from Scudder et al. (2014).

Step	Description
1	Label 30 ml acid cleaned Savillex Teflon digestion vessel using a Staedtler Lumo-color pen
2	Add 1 ml of concentrated nitric acid to each Teflon vessel
3	For each sample weigh out 0.0498-0.0502 g of powder, record the weight and pour into the Teflon vessel
4	Add additional 2 ml of concentrated nitric acid
5	Add 1 ml concentrated hydrochloric acid to each vessel. Seal tightly and let sit for 1 hour.
6	Add 1 ml concentrated hydrofluoric acid to each vessel. Seal very tightly and cook on hotplate, sub-boiling 24 hours.
7	Place vessel in ultrasonicator filled with water up to the level of the samples inside the Teflon vessels. Sonicate for 60 minutes.
8	Slowly (drop-by-drop) add 1 ml of hydrogen peroxide to each vessel, leave un-capped until samples stop reacting. Reseal and heat on hotplate for 5 hours.
9	Add another 1 ml of hydrogen peroxide to each vessel, reseal and heat on hotplate for up to 5 days or until sample is fully dissolved.
10	Uncap vessels and clean cap with deionized water and drain into vessel
11	Put open vessels on hotplate. Cook until samples are fully dried (~36 hours).
12	Add 1.2 ml of concentrated nitric acid to re-dissolve dried sample. Let sit for 5 hours and sonicate for 30 minutes.
13	Dilute to 60 g (approximately 1200x dilution)

Table S5. Wavelength and relative standard deviation shown for 10 elements analyzed by ICP-OES.

Ele-ment	ICP-OES Wave-length	2 rel. std. dev.
Ba	233 radial	± 4%
Ca	315 radial	± 2%
Fe	238.204	± 2%
Al	394.401	± 3%
Ti	337.279	± 2%
Mn	259.372	± 2%
Mg	285.213	± 2%
Sr	407.771	± 2%
K	766.49	± 3%
Si	212.412	± 16%

Dataset	Content
S1	Site 1209 bulk stable carbon and oxygen isotope data generated for this study and published elsewhere.
S2	Site 1210 bulk stable carbon and oxygen isotope data generated for this study and published elsewhere.
S3	Composite bulk stable carbon and oxygen isotope data generated for this study and published elsewhere.
S4	Site 1209 XRF data generated for this study.
S5	Site 1210 XRF data generated for this study.
S6	Composite XRF data generated for this study and published elsewhere.
S7	Offsets applied to cores from Holes 1209A, 1209B, 1209C.
S8	List of tie points used to create the revised composite depth section (rmcd) for Site 1209
S9	Mapping pairs for adjusting cores to the rmcd splice of Site 1209
S10	Offsets applied to cores from Holes 1210A and 1210B.
S11	List of tie points used to create the revised composite depth section (rmcd) for Site 1210
S12	Mapping pairs for adjusting cores to the rmcd splice of Site 1210
S13	Site-to-site correlation tie points between Sites 1210 and 1209 revised composite depth.
S14	Sites 1209 and 1210 barite and calcium carbonate data.
S15	Sites 1209 and 1210 bulk digestion and excess Ba data.
S16	Benthic foraminiferal data.

Supplement References

Batenburg, S. J., Sprovieri, M., Gale, A. S., Hilgen, F. J., Hüsing, S., Laskar, J., Liebrand, D., Lirer, F., Orue-Etxebarria, X., and Pelosi, N.: Cyclostratigraphy and astronomical tuning of the Late Maastrichtian at Zumaia (Basque country, Northern Spain), Earth Planet. Sci. Lett., 359, 264–278, 2012.

Batenburg, S. J., Gale, A. S., Sprovieri, M., Hilgen, F. J., Thibault, N., Boussaha, M., and Orue-Etxebarria, X.: An astronomical time scale for the Maastrichtian based on the Zumaia and Sopelana sections (Basque country, northern Spain), J. Geol. Soc., 171, 165–180, 2014.

Clark, K. R.: Late Campanian-Maastrichtian Planktic Foraminiferal Biostratigraphy, Taxonomy, and Isotope Paleoecology of ODP Leg 198 Sites 1209 and 1210, Shatsky Rise, MS Thesis, University of Massachusetts Amherst, 224 p., 2012.

Dameron, S. N., Leckie, R. M., Clark, K., MacLeod, K. G., Thomas, D. J., and Lees, J. A.: Extinction, dissolution, and possible ocean acidification prior to the Cretaceous/Paleogene (K/Pg) boundary in the tropical Pacific, Palaeogeogr. Palaeoclimatol. Palaeoecol., 485, 433–454, 2017.

Dymond, J., Suess, E., and Lyle, M.: Barium in deep-sea sediment: A geochemical proxy for paleoproductivity, Paleoceanography, 7, 163–181, 1992.

Eagle, M., Paytan, A., Arrigo, K. R., van Dijken, G., and Murray, R. W.: A comparison between excess barium and barite as indicators of carbon export, Paleoceanography, 18, 2003.

Jung, C., Voigt, S., and Friedrich, O.: High-resolution carbon-isotope stratigraphy across the Campanian–Maastrichtian boundary at Shatsky Rise (tropical Pacific), Cretac. Res., 37, 177–185, 2012.

Jung, C., Voigt, S., Friedrich, O., Koch, M. C., and Frank, M.: Campanian-Maastrichtian ocean circulation in the tropical Pacific, Paleoceanogr. Paleoclimatology, 28, 562–573, 2013.

Laskar, J., Robutel, P., Joutel, F., Gastineau, M., Correia, A., and Levrard, B.: A long-term numerical solution for the insolation quantities of the Earth, Astron. Astrophys., 428, 261–285, 2004.

Olivarez Lyle, A. and Lyle, M. W.: Missing organic carbon in Eocene marine sediments: Is metabolism the biological feedback that maintains end-member climates?, Paleoceanography, 21, 2006.

Paytan, A., Kastner, M., and Chavez, F.: Glacial to interglacial fluctuations in productivity in the equatorial Pacific as indicated by marine barite, Science, 274, 1355–1357, 1996.

Reitz, A., Pfeifer, K., De Lange, G., and Klump, J.: Biogenic barium and the detrital Ba/Al ratio: a comparison of their direct and indirect determination, Mar. Geol., 204, 289–300, 2004.

Scudder, R. P., Murray, R. W., Schindlbeck, J. C., Kutterolf, S., Hauff, F., and McKinley, C. C.: Regional-scale input of dispersed and discrete volcanic ash to the Izu-Bonin and Mariana subduction zones, Geochem. Geophys. Geosystems, 15, 4369–4379, 2014.